CHEMISTRY OF MATERIALS

Article

pubs.acs.org/cm

Multivalency-Induced Band Gap Opening at MoS_2 Edges

Michael C. Lucking,[†] Junhyeok Bang,[§] Humberto Terrones,[†] Yi-Yang Sun,[†] and Shengbai Zhang*,[†]

[†]Department of Physics, Applied Physics and Astronomy, Rensselaer Polytechnic Institute, Troy, New York 12180, United States

[§]Division of Materials Science, Korea Basic Science Institute (KBSI), Daejeon 305-806, Republic of Korea

Supporting Information

ABSTRACT: Zigzag edges of monolayer MoS_2 and other transition-metal (TM) dichalcogenides are experimentally shown to exhibit strong photoluminescence. Atomic models that have been proposed for these edges, however, are all metallic. Here, we address this puzzle by using first-principles calculations. We found that a more generic electron counting model (ECM) can be developed, which, when coupled with the ability of TM atoms at edges to change their valency from 4+ to 5+, can quantitatively account for the band gap opening at the zigzag edges. Due to the ECM, a 3× periodicity along the zigzag edge is necessary to open the band gap. Moreover, consistent with experiment, oxygen adsorption is shown to open even larger band gaps than intrinsic edges.

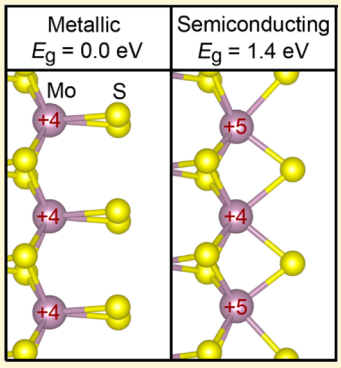

INTRODUCTION

Transition metal dichalcogenides (TMDs) such as MoS_2 have attracted considerable interest recently because of their unique properties and potential applications.[1] Carrier mobility up to 200 $cm^2\ V^{-1}\ s^{-1}$ at room-temperature and large band gap have been utilized to make field-effect transistors with large current on/off ratio and ultralow standby power dissipation.[2] Lateral (or in-plane) heterojunctions between TMD monolayers have been fabricated,[3,4] opening the door for fabrication of pure two-dimensional transistors. The existence of multivalley of the conduction band, which could be selectively populated by electrons (valley polarization), has led to a new research field dubbed valleytronics.[5−8] Moreover, the large exciton binding energy of 0.5−1 eV in TMDs[9,10] and the direct band gaps of the monolayer TMDs suggest that they might become important materials for next-generation optoelectronics.[11−13] Applications such as photovoltaics[14] and photocatalysis[15−17] have also been proposed.

Most aforementioned applications require the control of edge states. Metallic edges may allow leakage current, which is detrimental to device function. The armchair nanoribbons of MoS_2 have been theoretically shown to have a small gap (0.56 eV with the DFT-PBE approximation[18]), which can be further opened to 0.67 eV by hydrogen adsorption.[18−20] These values should be compared to 1.67 eV for monolayer MoS_2. However, armchair nanoribbons are usually not seen in experiment[21−24] because zigzag ribbons have considerably lower energies.[24,25] So far, theoretical calculations have shown that zigzag edges are metallic.[18−20,25−27] A transition to semiconducting behavior can only be induced by strain or applying an electric field yielding a tiny theoretical gap of 87 meV.[28] These results are at odds with experiments, showing strong photoluminescence (PL) from near-edge regions of TMD flakes,[11,29] which suggest that the zigzag edges may have also been passivated. Given this rapidly growing research field, it is urgently needed to develop a systematic understanding of the gap opening mechanism at the TMD zigzag edges.

In this paper, taking MoS_2 as a prototype, we address the issue whether TMD zigzag edges are metallic or semiconducting using first-principles calculations. We show that edge band gap opening is a multifaceted process that involves the following: (1) edge periodicity for reconstruction, which should be 3× (i.e., three bulk units along the edge), (2) the unique ability of TM atoms to change their valence states, and (3) oxygen presence. Taking the Mo edge as an example, PBE shows that unreconstructed 1× edge is metallic, 3× reconstruction opens the gap to 0.17 eV, multivalence increases the gap to 0.71 eV, and oxidation further increases the gap to 1.23 eV. Even for the S edge, a combined gap opening of 0.84 eV is achieved. These results can be contrasted to those of hydrogen passivated armchair edge (0.67 eV) and monolayer MoS_2 (1.67 eV). Clearly, multivalency of the TM is the key for significant gap opening without any chemical impurity such as oxygen.

METHODS

We use density functional calculation with the PBE functional[30] and the projected augmented wave (PAW) potential method[31] as implemented in the VASP code.[32] The PAW potentials for Mo and S include (4p, 4d, 5s) and (3s, 3p) electrons, respectively. The wave functions are expanded in a plane wave basis up to a cutoff energy of 300 eV. We use a supercell

Received: February 1, 2015
Revised: April 21, 2015
Published: April 23, 2015

DOI: 10.1021/acs.chemmater.5b00398
Chem. Mater. 2015, 27, 3326−3331

containing 11 zigzag chains, as shown in Figure 1a, to model zigzag edges. Approximately 15 Å of vacuum are used in the perpendicular directions. More than 16 Å of vacuum separate the edges from each other. We use (4 × 1 × 1) and (12 × 1 × 1) *k*-points to sample the Brillouin zone for the 3× and 1× supercells, respectively, which give rise to three and seven inequivalent k-points, respectively, along the periodic direction. The calculated lattice constant of 3.184 Å for the MoS_2 monolayer is used to set up the supercells. Spin-polarized calculations are performed. The atomic structures are relaxed until the forces are less than 0.01 eV/Å. All optimized atomic structures are provided in the Supporting Information. We do not consider edge excitons. Not only are the excitons computationally more challenging, they are such an important subject that warrants a separate investigation.

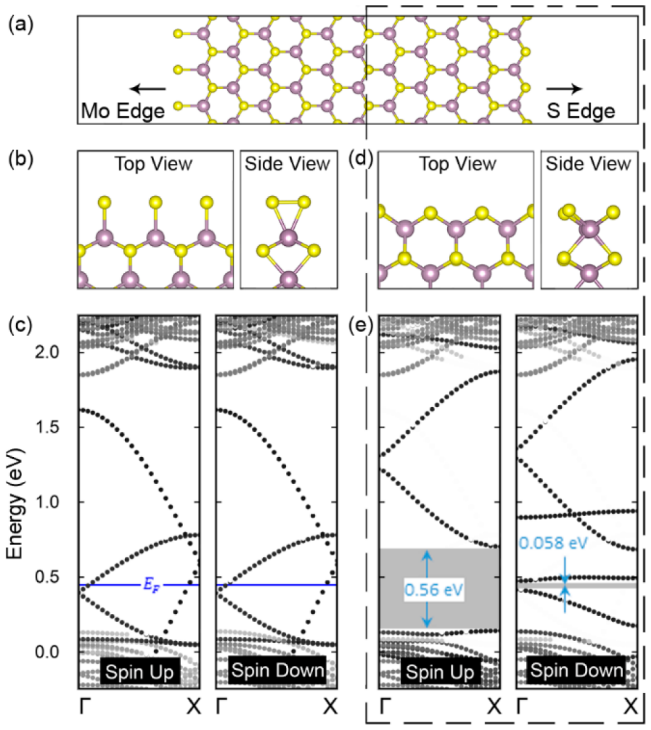

Figure 1. (a) Illustration of the supercell setup used for the calculations. Atomic (b) and band (c) structure of the pristine Mo edge terminated by S. Atomic (d) and band (e) structure of the pristine S edge. Mo atoms are shown in purple, and sulfur is shown in yellow. The grayscale in the band structure plots show the proximity of a state to the respective edge, where black represents bands localized near the edge of interest and white represents bands localized near the opposite edge. Fermi level is drawn in blue. The energy zero is set to the VBM of bulk monolayer. The shaded regions show the band gaps.

Electron Counting Model (ECM). For semiconductors, unpaired electrons at surface or edge dangling bonds should be avoided to maintain a band gap. The dangling bonds can be passivated by extrinsic atoms (e.g., by H atoms on Si surfaces) or self-passivated through reconstruction, whereby all the dangling bonds of the anions are doubly occupied (i.e., forming lone pairs), and all the dangling bonds of the cations are empty.[33] The electron counting model is successful in predicting reconstructions on the surfaces of most covalent semiconductors, especially for group III-V and most II-VI compounds. MoS_2 is, however, not a traditional semiconductor, for which the meaning of a covalent bond is not so clear. A more generic electron counting model is necessary to apply to a broader range of materials.

Our model makes use of the known chemistry of Mo and S in MoS_2, namely, each Mo donates (**4**) electrons to nearest neighbor S's, whereas each S accepts (**2**) electrons from nearest neighbor Mo's. Here, for clarity, we use bold parentheses for the number of electrons to be donated or accepted, underlined numbers for the number of neighboring atoms, and square bracket for the number of same type of atoms in the chemical formula. In (monolayer) bulk MoS_2, each Mo has $\underline{6}$ nearest neighbor S and each S has $\underline{3}$ nearest neighbor Mo. Thus, each Mo donates $(\mathbf{4})/\underline{6} = 2/3$ electrons to a neighboring S, and each S accepts $(\mathbf{2})/\underline{3} = 2/3$ electrons from a neighboring Mo. The net charge transfer within any bulk formula unit $MoS_{[2]}$ should be zero because $(\underline{6} \times (2/3) - [2] \times \underline{3} \times (2/3)) = 0$. Note that this charge balance does not apply to edges. One needs to balance the charge through edge reconstruction. With a fractional charge donating power of +2/3 per Mo bond and accepting power of −2/3 per S bond, the edge can only be fully compensated in a 3× periodicity or any of its multiples. Naturally, zigzag edges having 1× or 2× periodicity are always metallic, as reported previously.[18−20,25−27] A complete compensation tends to make the 3× edges thermodynamically stable. Similar findings have been reported previously for the zigzag edges of graphene.[34] The situation for armchair edges where Mo and S are present in stoichiometry is, however, different, as self-compensation can be automatically achieved without any reconstruction.

RESULTS AND DISCUSSION

Pristine Edges. We first consider the pristine edges with a 3× periodicity. Note that in the supercell approach, we can only calculate ribbons with two edges and the two for a zigzag ribbon are inequivalent: one is Mo-polar (or Mo edge in short), another is S-polar (or S edge), as illustrated in Figure 1a. It has been experimentally observed that the Mo edges are also terminated by S atoms.[21,35,36] We therefore define the pristine ribbons to have the Mo and S edges in Figures 1b and 1d, respectively; both are S terminated. It is, however, convenient to reference the Mo edge reconstruction back to ideal Mo termination. Hence, the pristine edge defined here is a $3S_2$ (ad-dimer) Mo edge. The calculated band structures of the pristine Mo and S edges are shown in Figures 1c and 1e, respectively. The band structures for the Mo and S edges can be separated by projecting the electronic states onto the edge atoms of the ribbon. We apply a grayscale to these plots according to the distance to the edge of interest, such that states at the other edge are all filtered out.

It can be seen from Figure 1c that even with the 3× periodicity, the pristine Mo edge is still metallic. The spins are nearly degenerate (i.e., nonspin-polarized) and two bands cross the Fermi level (E_F) at different points in the Brillouin zone. Figure 1b, side view, shows that the S atoms at the Mo edge move toward each other to form S_2 dimers. Different from the Mo edge, however, Figure 1e shows that the pristine S edge has a gap of 0.56 eV in the spin-up channel. However, the gap for the spin-down channel is only 0.06 eV. Because the S-covered Mo edges are most often seen in experiment,[21,36] determining its gap behavior can be critically important.

Open Band Gaps by Satisfying the ECM. For a 3× Mo edge, the ECM suggests that the three Mo atoms donate a total of $(3 \times \underline{2} \times (2/3)) = 4$ electrons to whatever S added onto the edge. For a 3× S edge, on the other hand, the three Mo atoms

DOI: 10.1021/acs.chemmater.5b00398
Chem. Mater. 2015, 27, 3326−3331

adjacent to edge S atoms donate to them $(3 \times \underline{4} \times (2/3)) = 8$ electrons. The S atoms are either a 2-electron acceptor (when remaining to be a single atom) or a 1-electron acceptor (when forming a S_2 dimer). The latter happens because by sharing 1 electron in a covalent S−S bond, each S atom in the S_2 dimer effectively only needs 1 more electron.

Consider now the pristine $3S_2$ Mo edge. One may use pseudo-H atoms, each has 2/3 electrons, to passivate the edge. Upon hydrogenation, however, all the dimers are broken, leaving behind with six S atoms. As discussed, the Mo atoms donate 4 electrons, whereas the six S atoms need to accept 12 electrons, leaving a deficiency of 8. By having two pseudo-H per S (see Figure S1 in Supporting Information), one can make up for the difference of $(6 \times 2 \times (2/3)) = 8$ electrons. Our PBE calculation indeed shows that such a Mo edge has a gap of about 0.25 eV, suggesting the applicability of the ECM. Next, consider a more realistic structure without the pseudo-H (i.e., the 2S edge). Again, the Mo atoms donate 4 electrons. One needs two S adatoms (see Figure 2a) to fulfill the ECM. Figure 3a shows the spin-degenerate band structure for this model. Although the ECM works, the band gap of 0.17 eV is evidently too small (see Figure 3a).

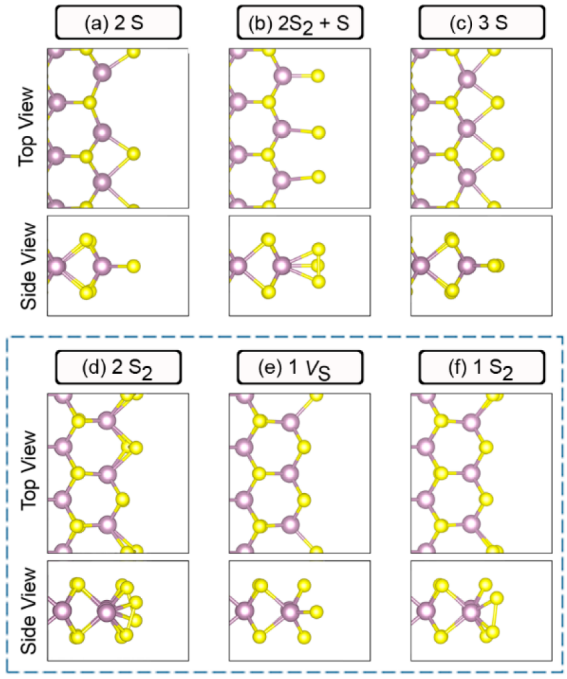

Figure 2. Atomic structures (top and side view) of the Mo (a,b,c) and S (d,e,f) edge reconstructions. At the Mo edge, the reconstructions are named according to the number of S atoms and/or S dimers (S_2) added to the Mo terminated edge. At the S edge, there are three pairs of S atoms at the edge. The model names, $2S_2$ and $1S_2$, mean that two and one pair of S atoms, respectively, at the edge come close to each other forming dimers, while the model $1V_S$ means that one S atom is removed from the edge forming a S vacancy (V_S).

Similar analysis applies to the S edge. Here, the Mo atoms donate 8 electrons. There are 6 edge S atoms, which need to accept 12 electrons. Placing one pseudo-H (with 2/3 electrons) on each edge S atom (Figure S1 in Supporting Information) makes up for the difference of $(6 \times (2/3)) = 4$ electrons, so ECM is satisfied. Our PBE calculation shows a gap opening of 0.30 eV. Forming two S_2 dimers at the S edge (see Figure 2d) is another possibility, because the remaining two S atoms accept 4

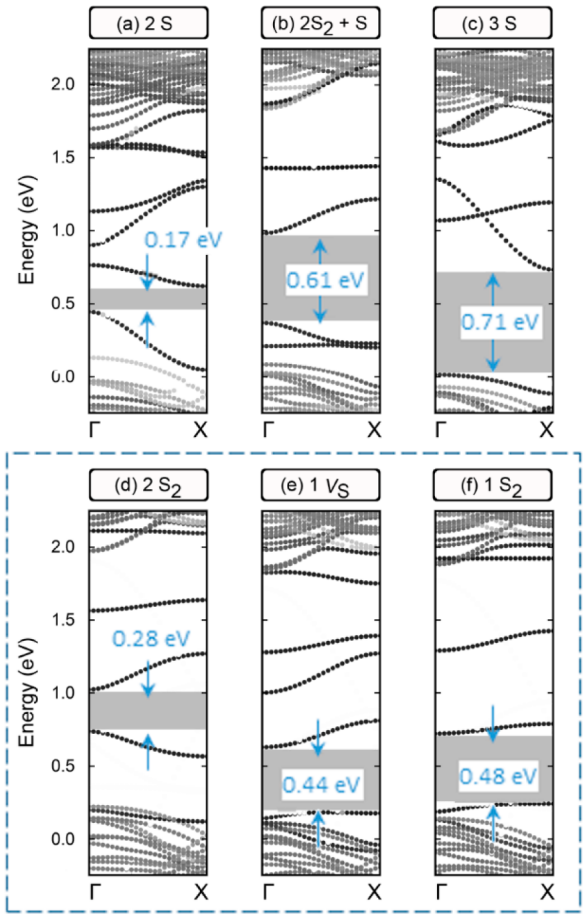

Figure 3. Band structure of the Mo (a,b,c) and S (d,e,f) edges shown in Figure 2. The band gap regions are shaded in gray. There is no spin-polarization for all structures except for the $2S_2$ model at the S edge, for which only the spin-up component is shown, while the band gap in the spin-down component is larger (0.54 eV).

electrons, whereas the two dimers accept also 4 electrons. The total number of accepted electrons is 8, which matches the donated electrons and hence ECM is fulfilled. Figure 3d shows that $2S_2$ has a band gap of 0.28 eV.

Multivalency That Opens Larger Band Gap. The band gaps opened by the ECM are generally small and may not be enough to account for experimental observations. We note that Mo is a transition metal which could also exist in valence 5+ or 6+, depending on the local chemical environment. A change of the valency (or multivalence) may thus happen at edges. This, coupled with the ECM, may account for the gap opening. Here, we consider the case in which there is a 2-electron deficiency at edges. To make the balance, either two Mo must change their valence from 4+ to 5+ or one Mo must change its valence from 4+ to 6+.

Let us first reconsider the Mo edge. Figure 2b shows a $(2S_2 + S)$ reconstruction with two S_2 addimers and one S adatom. The three Mo atoms donate 4 electrons, whereas the two S_2 plus the S need to accept $2 \times 2 + 2 = 6$ electrons leaving a deficiency of 2. Figure 3b shows that the $(2S_2 + S)$ model has a significantly larger band gap of 0.61 eV. Figure 2c shows, as an alternative, a 3S reconstruction where three S adatoms are placed at ideal Mo edge. Again, the Mo atoms donate 4 electrons, whereas the three S need to accept 6 electrons resulting in a deficiency of 2. Figure 3c shows that 3S has an even larger band gap of 0.71 eV

DOI: 10.1021/acs.chemmater.5b00398
Chem. Mater. 2015, 27, 3326−3331

(the largest for intrinsic Mo edge). Using a hybrid HSE functional, a 1.4 eV gap is obtained for the 3S structure. We notice that, for monolayer MoS_2, the HSE gap of 2.2 eV is still substantially smaller than the GW gap of ~2.8 eV,[9,37] so the actual gap for the edge may also be larger than 1.4 eV.

For the S edge, Figure 2e shows a V_S reconstruction where an edge S atom is removed. Here, the Mo atoms donate 8 electrons. With one S vacancy, 5 edge S atoms remain to accept $5 \times 2 = 10$ electrons, leading to a deficiency of 2. Figure 3e shows that V_S has a band gap of 0.44 eV. Figure 2f shows a S_2 reconstruction, as an alternative to V_S. Here, instead of S removal, one of the edge S pairs forms a dimer. The four remaining S plus 1 S_2 can accept $4 \times 2 + 2 = 10$ electrons, leading again to a deficiency of 2. Figure 3f shows that this structure has a band gap of 0.48 eV. Using a hybrid HSE functional, a 1.1 eV band gap is obtained for the S_2 reconstruction. We have calculated a large number of possible reconstructions and the above examples are only those with low edge energies (see Figure 4). They are all in support of the Mo multivalency picture within the ECM.

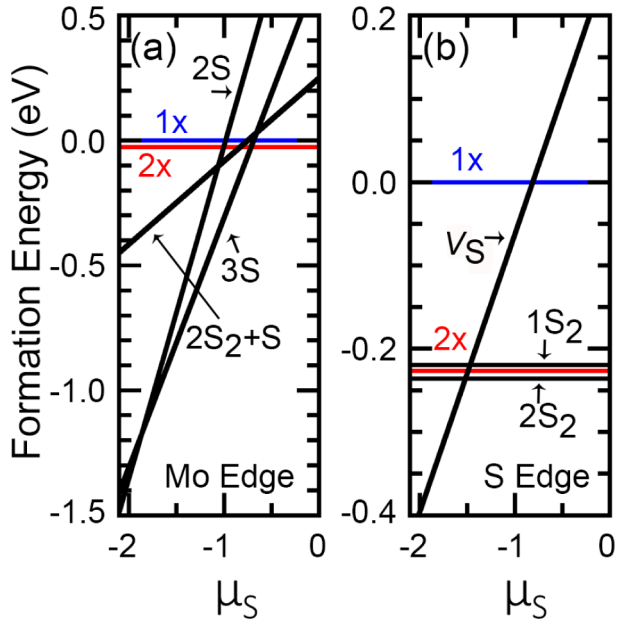

Figure 4. Formation energy of the different (a) Mo and (b) S edges per 1× unit. The 1× structure for both the Mo and S edges are shown in Figure 1a. In the 2× structure, both S pairs at the Mo edge form dimers, while only one of the two S pairs at the S edge forms a dimer.

Before moving on, we would like to answer: do two Mo atoms change their valency from 4+ to 5+ or one Mo atom changes its valency from 4+ to 6+? To do so, we may replace Mo by Zr, the element which exists, in most cases, only in valence 4+. By substituting either one or two Mo by Zr in a 3× edge, we can tell whether the remaining edge Mo atom(s) are valence 5+ or 6+ by examining the gap opening. We find that only one Zr per 3× opens the gap (see Figure S2 in Supporting Information), which confirms that those edge Mo, which has changed valency, change from 4+ to 5+, not 6+.

Thermodynamic Stability. The formation energies of various edges are shown in Figure 4, as a function of S chemical potential. The formation energy is calculated as the difference in total energies between the ribbon of interest and the pristine ribbon. Negative energies represent more stable edges than pristine edges. The energies are normalized to per unit cell length (1×). The chemical potential of S is referenced to S_2 molecule. The chemical potential is subject to the constraint, $\mu_{Mo} + 2\,\mu_S < \Delta H(MoS_2)$, where $\Delta H(MoS_2)$ is the enthalpy of formation of MoS_2.[38]

At the Mo edge, the metallic edge in Figure 1b with a 2× periodicity is most stable for $\mu_S > -0.69$ eV (S-rich), because this edge contains the most S. This may explain why metallic edges have also been observed in experiment.[21,22,26] When μ_S is reduced to below −0.69 eV, however, the semiconducting 3S edge (Figure 2c) becomes most stable. At the more S poor condition ($\mu_S < -1.89$ eV), however, the most stable edge changes to 2S with a significantly smaller gap. At the S edge, for a significant part of the S chemical potential, the smaller-gap $2S_2$ edge (Figure 2d) is most stable. In the S poor region ($\mu_S < -1.52$ eV), however, the larger-gap V_S edge is more stable. The S edge is always in favor of the 3× periodicity.

Effect of Mixed Edge Structures. In reality, the edges could be a mixture of different structures. To investigate this effect, we have calculated the band gap for a ribbon with 50% $2S_2$ + S and 50% 3S for the Mo edge and 50% 1 V_S and 50% S_2 for the S edge. We find a gap of 0.20 eV. This can be understood by examining the results in Figures 3b,c,e,f, where the band edge positions are all with respect to a common vacuum level. By taking the difference between the highest VBM and the lowest CBM, we obtain a gap of 0.22 eV. This is in good agreement with the direct calculation. In near equilibrium condition, Figure 4 suggests that one structure (e.g., 3S for the Mo edge) will dominate. Then the gap will be that of 3S, while other structures would produce localized gap states, whose level positions may be estimated similarly using Figure 3.

Effect of Oxygen Adsorption. Oxygen has recently been shown to be important in the observed strong photoluminescence at edges of monolayer MoS_2.[29] Here, we consider its effect on the largest-gap edges, namely, the 3S Mo edge and S_2 S edge. Our calculation shows that O_2 dissociate. Once dissociated, the O atom binds to S, not Mo. At the Mo edge, it binds to the second S rows from the edge, two O for every three S (see Figure 5a). The O adsorption shifts the CBM up by 0.31 eV and the VBM down by 0.20 eV. Figure 5b shows that the PBE band gap is increased from 0.71 to 1.23 eV. At the S edge, on the other hand, the O binds to the first (edge) S rows, also two O for every three S (see Figure 5c), leaving the S_2 dimer intact. Figure 5d shows that the PBE band gap is increased from 0.48 to 0.84 eV, mostly from an uplifting of the CBM. HSE calculations yield a 1.8 eV gap at the Mo edge and a 1.6 eV gap at the S edge. We can understand the existence of a band gap here by the ECM: an S or O is a 2-electron acceptor; as discussed earlier, an S_2 and SO dimer is also a 2-electron acceptor. Hence, the electron counting for the 3S and S_2 edge reconstructions holds after O adsorption. It is expected that the larger electronegativity of the oxygen further opens the band gap.

Tungsten Disulfide. WS_2 is another TMD that has also attracted considerable attention. We have calculated a WS_2 ribbons constructed by replacing all the Mo atoms in our largest-gap ribbon (3S Mo edge + S_2 S edge) by W. The band structure after structure optimization (Figure S3 in Supporting Information) is similar to that of MoS_2, so we expect our analysis here to hold for other TMDs.

DOI: 10.1021/acs.chemmater.5b00398
Chem. Mater. 2015, 27, 3326−3331

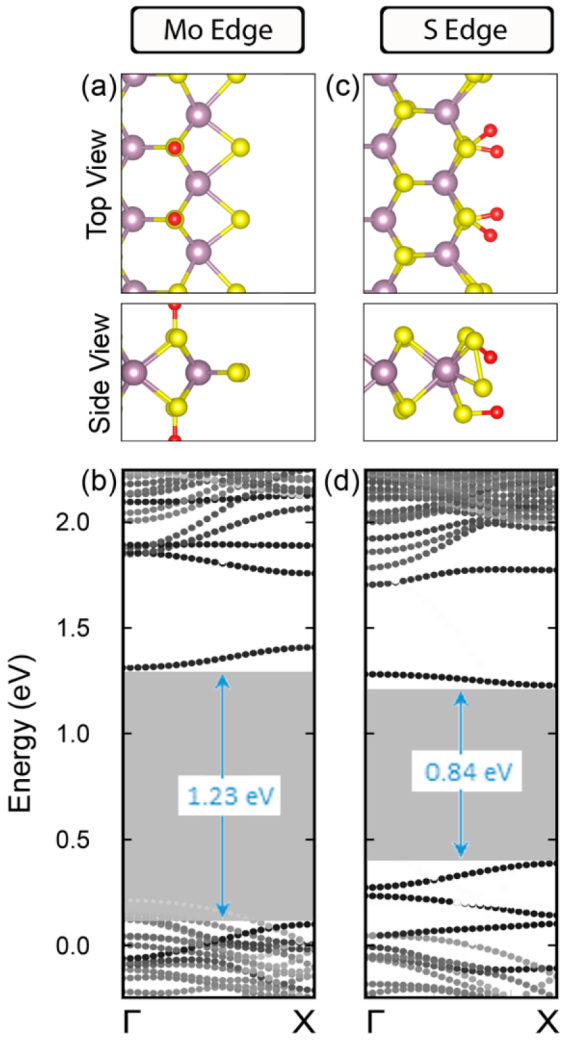

Figure 5. Atomic and band structures of Mo (a,b) and S (c,d) edges from Figure 2c and 2f, respectively, after O adsorption.

CONCLUSIONS

In summary, using first-principles calculations, we solved the puzzle of whether the zigzag edge of monolayer MoS_2 is metallic or semiconducting. The answer in fact depends sensitively on S chemical potential and the polarization of the edges. We developed a more generic electron counting model, which allows us to determine the 3× periodicity as the fundamental unit for semiconducting edges. We also demonstrated that the multivalency of Mo atoms is a critical factor for the reconstruction of the edges to fulfill the ECM and to further open the band gap. In addition, consistent with experiments, oxygen adsorption at edges results in even larger band gaps than the intrinsic edges. Finally, our results can be extended to other TMD not only semiconducting, based on transition metal (Mo,W) and selenium or tellurium, but the results can also be applied to metallic compounds such as NbS_2 and $NbSe_2$, thus opening different possibilities for band gap engineering at the edges.

ASSOCIATED CONTENT

Supporting Information

Atomic and band structures for fractional H-passivated edges, WS_2 edges and Zr-substituted edges. Optimized atomic coordinates for the edge structures shown in Figures 1, 2, and 5. The Supporting Information is available free of charge on the ACS Publications website at DOI: 10.1021/acs.chemmater.5b00398.

AUTHOR INFORMATION

Corresponding Author

*Email: zhangs9@rpi.edu.

Notes

The authors declare no competing financial interest.

ACKNOWLEDGMENTS

This work is supported by US Department of Energy (DOE) under Grant No. DE-SC0002623. The supercomputer time was provided by the National Energy Research Scientific Computing Center (NERSC) under DOE Contract No. DE-AC02-05CH11231 and the Center for Computational Innovations (CCI) at Rensselaer Polytechnic Institute.

REFERENCES

(1) Jariwala, D.; Sangwan, V. K.; Lauhon, L. J.; Marks, T. J.; Hersam, M. C. *ACS Nano* **2014**, *8*, 1102.
(2) Radisavljevic, B.; Radenovic, A.; Brivio, J.; Giacometti, V.; Kis, A. *Nat. Nanotechnol.* **2011**, *6*, 147.
(3) Huang, C.; Wu, S.; Sanchez, A. M.; Peters, J. J. P.; Beanland, R.; Ross, J. S.; Rivera, P.; Yao, W.; Cobden, D. H.; Xu, X. *Nat. Mater.* **2014**, *13*, 1096.
(4) Gong, Y.; Lin, J.; Wang, X.; Shi, G.; Lei, S.; Lin, Z.; Zou, X.; Ye, G.; Vajtai, R.; Yakobson, B. I.; Terrones, H.; Terrones, M.; Tay; Beng, K.; Lou, J.; Pantelides, S. T.; Liu, Z.; Zhou, W.; Ajayan, P. M. *Nat. Mater.* **2014**, *13*, 1135.
(5) Xiao, D.; Liu, G.-B.; Feng, W.; Xu, X.; Yao, W. *Phys. Rev. Lett.* **2012**, *108*, 196802.
(6) Mak, K. F.; He, K.; Shan, J.; Heinz, T. F. *Nat. Nanotechnol.* **2012**, *7*, 494.
(7) Behnia, K. *Nat. Nanotechnol.* **2012**, *7*, 488.
(8) Zeng, H.; Dai, J.; Yao, W.; Xiao, D.; Cui, X. *Nat. Nanotechnol.* **2012**, *7*, 490.
(9) Ramasubramaniam, A. *Phys. Rev. B* **2012**, *86*, 115409.
(10) Ugeda, M. M.; Bradley, A. J.; Shi, S.-F.; da Jornada, F. H.; Zhang, Y.; Qiu, D. Y.; Ruan, W.; Mo, S.-K.; Hussain, Z.; Shen, Z.-X.; Wang, F.; Louie, S. G.; Crommie, M. F. *Nat. Mater.* **2014**, *13*, 1091.
(11) Gutiérrez, H. R.; Perea-López, N.; Elías, A. L.; Berkdemir, A.; Wang, B.; Lv, R.; López-Urías, F.; Crespi, V. H.; Terrones, H.; Terrones, M. *Nano Lett.* **2012**, *13*, 3447.
(12) Liu, H.; Neal, A. T.; Ye, P. D. *ACS Nano* **2012**, *6*, 8563.
(13) Radisavljevic, B.; Kis, A. *Nat. Mater.* **2013**, *12*, 815.
(14) Bernardi, M.; Palummo, M.; Grossman, J. C. *Nano Lett.* **2013**, *13*, 3664.
(15) Kibsgaard, J.; Chen, Z.; Reinecke, B. N.; Jaramillo, T. F. *Nat. Mater.* **2012**, *11*, 963.
(16) Jaramillo, T. F.; Jørgensen, K. P.; Bonde, J.; Nielsen, J. H.; Horch, S.; Chorkendorff, I. *Science* **2007**, *317*, 100.
(17) Morales-Guio, C. G.; Tilley, S. D.; Vrubel, H.; Gratzel, M.; Hu, X. *Nat. Commun.* **2014**, *5*, 3059.
(18) Pan, H.; Zhang, Y.-W. *J. Mater. Chem.* **2012**, *22*, 7280.
(19) Botello-Méndez, A. R.; López-Urías, F.; Terrones, M.; Terrones, H. *Nanotechnology* **2009**, *20*, 325703.
(20) Ataca, C.; Şahin, H.; Aktürk, E.; Ciraci, S. *J. Phys. Chem. C* **2011**, *115*, 3934.
(21) Lauritsen, J. V.; Kibsgaard, J.; Helveg, S.; Topsoe, H.; Clausen, B. S.; Laegsgaard, E.; Besenbacher, F. *Nat. Nanotechnol.* **2007**, *2*, 53.
(22) Helveg, S.; Lauritsen, J. V.; Lægsgaard, E.; Stensgaard, I.; Nørskov, J. K.; Clausen, B. S.; Topsøe, H.; Besenbacher, F. *Phys. Rev. Lett.* **2000**, *84*, 951.
(23) Hansen, L. P.; Ramasse, Q. M.; Kisielowski, C.; Brorson, M.; Johnson, E.; Topsøe, H.; Helveg, S. *Angew. Chem., Int. Ed.* **2011**, *50*, 10153.

DOI: 10.1021/acs.chemmater.5b00398
Chem. Mater. 2015, 27, 3326−3331

(24) Wang, Z.; Li, H.; Liu, Z.; Shi, Z.; Lu, J.; Suenaga, K.; Joung, S.-K.; Okazaki, T.; Gu, Z.; Zhou, J.; Gao, Z.; Li, G.; Sanvito, S.; Wang, E.; Iijima, S. *J. Am. Chem. Soc.* **2010**, *132*, 13840.
(25) Li, Y.; Zhou, Z.; Zhang, S.; Chen, Z. *J. Am. Chem. Soc.* **2008**, *130*, 16739.
(26) Bertram, N.; Cordes, J.; Kim, Y. D.; Ganteför, G.; Gemming, S.; Seifert, G. *Chem. Phys. Lett.* **2006**, *418*, 36.
(27) Seivane, L. F.; Barron, H.; Botti, S.; Lopes Marques, M. A.; Rubio, Á.; López-Lozano, X. *J. Mater. Res.* **2013**, *28*, 240.
(28) Kou, L.; Tang, C.; Zhang, Y.; Heine, T.; Chen, C.; Frauenheim, T. *J. Phys. Chem. Lett.* **2012**, *3*, 2934.
(29) Nan, H.; Wang, Z.; Wang, W.; Liang, Z.; Lu, Y.; Chen, Q.; He, D.; Tan, P.; Miao, F.; Wang, X.; Wang, J.; Ni, Z. *ACS Nano* **2014**, *8*, 5738.
(30) Perdew, J. P.; Burke, K.; Ernzerhof, M. *Phys. Rev. Lett.* **1996**, *77*, 3865.
(31) Blöchl, P. E. *Phys. Rev. B* **1994**, *50*, 17953.
(32) Kresse, G.; Furthmüller, J. *Comput. Mater. Sci.* **1996**, *6*, 15.
(33) Pashley, M. D. *Phys. Rev. B* **1989**, *40*, 10481.
(34) Sun, Y. Y.; Ruan, W. Y.; Gao, X.; Bang, J.; Kim, Y.-H.; Lee, K.; West, D.; Liu, X.; Chan, T. L.; Chou, M. Y.; Zhang, S. B. *Phys. Rev. B* **2012**, *85*, 195464.
(35) Bollinger, M. V.; Jacobsen, K. W.; Nørskov, J. K. *Phys. Rev. B* **2003**, *67*, 085410.
(36) Bollinger, M. V.; Lauritsen, J. V.; Jacobsen, K. W.; Nørskov, J. K.; Helveg, S.; Besenbacher, F. *Phys. Rev. Lett.* **2001**, *87*, 196803.
(37) Qiu, D. Y.; da Jornada, F. H.; Louie, S. G. *Phys. Rev. Lett.* **2013**, *111*, 216805.
(38) Zhang, S. B.; Northrup, J. E. *Phys. Rev. Lett.* **1991**, *67*, 2339.

DOI: 10.1021/acs.chemmater.5b00398
Chem. Mater. 2015, 27, 3326−3331